Comprehensive Status Report: November 18, 2004

OTRC Reliability of Mooring Systems for Floating Production Systems
MMS Project: 423 TO: 18203
PI's: Jun Zhang & Robert Gilbert
MMS COTR: A. Konczvald

This report provides a comprehensive summary of the research completed in all prior Phases of this project (September 2001 – August 2004), and describes research being done in the present Phase (September 2004 – August 2005) to complete this project.

Reliability of Mooring Systems for Floating Production Systems

Jun Zhang & Robert Gilbert

I. Objective & Introduction

Mooring systems for floating production systems, consisting individual mooring lines and anchors, are currently designed on the basis of individual components. The most heavily loaded line and anchor are checked under extreme loading conditions (hurricanes and loop currents) with the system of lines intact and with one line removed. However, the performance of the floating production system depends more directly on the performance of the system of lines and anchors rather than on the performance of a single line or anchor. This project is to assess and study the component and system reliabilities for the mooring system of a Spar that is representative of those being used today in the Gulf of Mexico.

A numerical code, COUPLE, was employed to compute global motions and tensions in the mooring lines given met-ocean conditions. There are two major computational codes involved in COUPLE. The first is for computing the specified wave, current and wind loads on the hull and the second deals with the loads and dynamics of the mooring/tendon/riser system. These two independent codes are coupled together by matching the forces and displacements of a mooring/tendon/riser system and the hull at their joints following prescribed connection conditions. The code for computing dynamics of the mooring/tendon/riser system is based on a slender-body assumption and employs a nonlinear Finite Element Method (FEM), known as CABLE3D. For this study, the original code was extended to accommodate for the large elongations in polyester lines and to model the scenario where an anchor pulls out and the line remains intact.

The reliability analyses were conducted using realistic probabilistic descriptions of the extreme met-ocean conditions (hurricanes and loop currents) for the Gulf of Mexico. Probabilities of failure during a 20-year design life were calculated for individual components and for the mooring system. A system failure with respect to station keeping was defined as the failure of two or more lines. Individual sequences of line breakage and

anchor pullout were considered to identify the most likely modes of failure in extreme conditions and to quantify redundancy in the mooring system.

A spar originally developed by the industry consortium, Deepstar, was chosen as the study spar, to be representative of technology in the Gulf of Mexico for water depths from 3,000 to 10,000 feet. It is a classic spar with steel mooring lines in 3,000 feet of water and polyester mooring lines in deeper depths. Although the project is based on the analysis of mooring systems of a Spar, the major results and the procedures for reliability analyses produced in this project may provide valuable guidance for the design of mooring system of other deep-water floating structures.

II. Coupled Analysis for the Interaction between a Hull and Its Mooring System: COUPLE

A numerical code developed recently, known as COUPLE, is especially effective and relatively simple in predicting dynamic interactions between a spar and its mooring/riser systems. Initially, it was developed for computing the 3-DOF (Degree-Of-Freedom) motions of a spar positioned by taut mooring lines using a quasi-static analysis (Cao and Zhang 1997) and later extended to allow for dynamical interaction between a spar and its mooring system to quantify the damping effects of a mooring system on the slow-drift motion of a spar (Chen et. al. 2001a). More recently, it was extended to allow for 6-DOF motions of a moored structure. COUPLE consists of two basic computational parts: one for computing the dynamics of a mooring/tendon/riser system and the other for the wave/current/wind loads on a moored floating structure (hull). The two independent codes are coupled by matching the forces and displacements of a mooring/tendon/riser system and the hull at their joints following prescribed connection conditions. The code for computing dynamics of the mooring/riser system is based on a slender-body assumption and employs a nonlinear Finite Element Method (FEM), known as CABLE3D (Ma and Webster, 1994). The computation in the original CABLE3D assumes infinitesimal elongation of a slender rod. Because large elongation slender components, such as springs and polyester ropes are often, respectively, used in a model test and a prototype mooring system, CABLE3D was extended to allow for large elongation in a mooring line to achieve accurate simulation (Chen et al. 2001b). The computation of nonlinear wave forces on a floating structure is accomplished by using either a second-order diffraction wave theory (such as WAMIT) and/or the Morison Equation. In the case of a spar, both potential and drag wave loads are computed using the Morison equation.

2.1 Wave, current and wind loads on hull

The total met-ocean environmental loads on an offshore structure can be divided into three major parts according to their origins which are denoted by the subscripts.

$$\mathbf{F} = \mathbf{F}_{Wave} + \mathbf{F}_{Current} + \mathbf{F}_{Wind}$$

The hull of a classical spar or the upper portion of a truss spar is virtually a cylinder. In using the Morison equation to compute wave and current loads, the normal force per unit

length on a cylinder of uniform diameter D is a function of the added mass coefficient, C_m, the drag coefficient, C_D, the density of water ρ_f, and the water particle velocity and acceleration. Water particle velocity and acceleration are the superposition of those of currents and waves. In the presence of ocean currents, wave frequencies may be shifted due to the Doppler Effect, which is neglected in our computation because it is assumed that current velocity is small in comparison with the phase velocity of incident waves.

Forces applied on the truncated bottom of a cylinder in the axial direction include the integration of wave pressure over the bottom S_B, and drag and added-mass forces which are equivalent to an half of a thin circular disk of the same diameter of the cylinder in heave motion (Sarpkaya and Isaacson, 1981). Wave kinematics and first- and second-order incident wave potential used in the computations are computed using a HWM (Zhang et al., 1996).

In order to account for Vortex Induced Motion (VIM) of a spar in the presence of strong currents, such as loop currents in the Gulf of Mexico, an additional term representing the lifting force (or transverse force) applied on per unit length on the cylinder is added into the Morison equation. This lifting force is a function of the lifting coefficient and the Strouhal Number, S_O. The Strouhal number and lifting coefficient in the context of a spar equipped with helical strakes on its surface and constrained by its mooring/riser systems are not well documented. In our computation, they were calibrated by fitting the mean, and the average 1/3rd and 1/5th amplitude and period of the simulated and measured LF sway of a spar model. The procedure for determining the lifting coefficient is detailed in Ding et. al. (2003).

Considering that the diameter of a spar, the velocities of currents and waves may change along its axis, the total wave and current loads on the spar are computed through the numerical integration of the corresponding loads over a number of segments along its longitudinal axis.

The computation of wind force is based on the empirical formula recommended by API (RP-2A), and is a function of the density of air, ρ_a, the shape coefficient, C_s, the total wind velocity, V_a, and the projected areas of the spar above sea level, A.

2.2 Hull Motions

Hull motions are computed from the forces acting on the hull using equations of linear motion for a rigid body. The forces include the loads from wave, wind and current, the hydrostatic restraining force, and the restraining force from mooring lines and risers.

2.3 Line Tensions

Computation of the motion and tension for a mooring line mainly follows Garrett (1982). To allow for large extension elements, such as springs or polyester ropes, Chen et al. (2001b) extended his formulation. A non-linear finite element method, called CABLE3D, is used to solve the dynamic and constraint equations

Because the modulus of a polyester rope depends on the tension, an empirical formula given by Del Vecchio (1992) is employed. Even at the mean position of a spar experiencing steady wind, current and wave loads, the modulus of polyester ropes in different mooring lines of an integrated mooring system is different because of different mean tensions. To determine the modulus of each mooring line, we first set the amplitude of dynamic tension to zero and calculate the modulus and tension of each polyester rope through iteration. Our experience indicates that the mean (static) tension and modulus of each mooring line converge rapidly just after two to three iterations. Based on the updated modulus of each rope, the simulation of the motion of a moored spar and the tension in mooring lines is made given the met-ocean conditions. Since the dominant responses of a spar are its low-frequency motions, the amplitude of dynamic tension in a polyester mooring line is also dominated by the corresponding low-frequency tension. Using a low-pass filter, the average amplitude of dynamic tension in a polyester rope can be determined. Knowing the approximate amplitude of dynamic tension, the modulus of each polyester line is updated and the dynamic simulation of a spar positioned by an integrated polyester mooring system is repeated. The iteration terminates if the relative difference in the modulus of two consecutive iterations is smaller than a prescribed error tolerance. More detailed description of the iterative procedure for determining the modulus of polyester mooring lines is given by Kim et. al. (2003).

2.4 Coupling between Hull and Mooring System

Motion equations for a hull and its mooring and riser systems are coupled by imposing prescribed conditions at their connections (fairleads or porches). For example, if a hinge connection is imposed between the hull and its mooring lines, then the forces and displacements of the hull and a mooring line at its fairlead are the same and no moment is applied there. More complicated connection conditions can be simulated by appropriately imposing force, moment, and relative displacement on the hull and its mooring/riser systems at their connections. The coupled equations for the hull and its mooring and riser systems are then solved simultaneously in the time domain using a Newmark-β method. At each time step, the velocities and positions of the hull and all mooring lines/risers are first predicted based on the velocities, positions and accelerations in the previous step. Then the required corrections for positions, velocities and accelerations are calculated based upon the dynamic equations. If the difference between the two corrections of consecutive iterations is less than a prescribed error tolerance, the simulation moves forward to the next step.

2.5 Numerical simulation of met-ocean environments

As an input to COUPLE, an incident ocean wave can be described by either time series of measured wave elevation or a free (linear) wave spectrum. For the comparison of simulated motion and forces of a floating structure with the corresponding measurements in the field or laboratories, measured wave elevations are often used as the input. The amplitude and initial phase of free waves in a measured irregular long-crested wave train are calculated as a function of frequency using the decomposition part of a HWM. The

amplitude and initial phase of free waves are then used in the prediction part of the same HWM for computing wave kinematics along the longitudinal axis of a spar as a function of time (Zhang et. al. 1996, Cao and Zhang 1997). In this work, long-crested incident waves were generated as input according to a JONSWAP spectrum with a sharp factor of 3.3. The related free wave spectrum is obtained by match its resultant spectrum (including bound waves) with a given analytic wave spectrum selected for the simulation. The amplitude of free waves and their initial phase are obtained using a random phase method (Tuah and Hudspeth 1982) based on a free-wave amplitude or energy spectrum.

The gustiness of wind is simulated based on a spectral energy density recommended by API rules (RP-2A). Based on a wind spectral density function, the total wind velocity is calculated following the procedures similar to those for simulating random water waves.

In the current version of COUPLE, both velocity and direction of currents are the input, which is a function of the vertical coordinate, *z*, but assumed to be steady. However, the extension to allow for unsteady currents can be made without principle difficulties.

III. Description of Theme Spar and Mooring System

In this project, COUPLE is used to simulate the global motions of a classical spar and tensions of its mooring lines deployed in 3,000, 6,000 and 10,000 ft water, respectively. The characteristics of the spar studied here are those of the DeepStar spar, a classical spar. The main characteristics of the hull are given in Table 3.1. The mooring systems deployed in all water depths consist of fourteen spread mooring lines as depicted in Figure 3.1. The differences between the three mooring system are the length and material of mooring lines. The mooring lines in 3,000 ft water are the traditional combination of steel chain-wire-chain, while those in 6,000 and 10,000 ft water are the integration of steel chain-polyester rope-steel chain. Their characteristics are given in Table 3.2. An example set of offset curves are plotted in Figures 3.2 for the 10,000-foot water depth. To demonstrating the necessity of using the extended CABLE3D based on the large elongation formulation, also plotted in the figure is the corresponding curve computed using the similar code but based on the small elongation assumption. The difference between the related offset curves of the integrated polyester mooring system is significant. The difference increases as water depth increases because elongation increases with water depth. Near the mean position (~ 17.5m) of the spar experiencing a 100-year hurricane in the Gulf of Mexico, the restraining force of the mooring system is reduced by about 20 % when elongation of polyester lines is included (Figure 3.2)

Table 3.1. Hull specifications.

Displacement	53600 metric ton
Total displacement	220640 metric ton
Diameter	122 ft
Length	705 ft
Draft	650 ft
Hard tank depth	220 ft
KB	540 ft
KG	462 ft
KG (based on total displacement)	314 ft

Radius of gyration	Pitch=221ft, yaw=28.5 ft
Drag force coefficient	1.16
Wind force coefficient	0.0558 (kips/(ft/sec)^2)
Center of pressure	722 ft ABL

Table 3.2. Mooring system specifications.

Water depth	3000 ft	6000 ft	10000 ft
Mooring type	Steel semi taut	Poly taut	Poly taut
Mooring pattern	14 point taut-leg omni-directional spread	14 point taut-leg omni-directional spread	14 point taut-leg omni-directional spread
Mooring line composition	Platform section 250'x5-1/4" K4 Studless chain	Platform section 300'x4.625" K4 Studless chain	Platform section 300'x5-1/8" K4 Studless chain
	Middle section 3,200'x5-3/8" Sheathed Wire	Middle section 7,800'x8.27" Polyester	Middle section 13,300'x9.06" Polyester
	Ground section 1150'x5-1/4" K4 Studless chain	Ground section 400'x4.625" K4 Studless chain	Ground section 400'x5-1/8" K4 Studless chain
Fairlead location	300 ft ABL	300 ft ABL	300 ft ABL
Pretension	680 kips	530 kips	650 kips

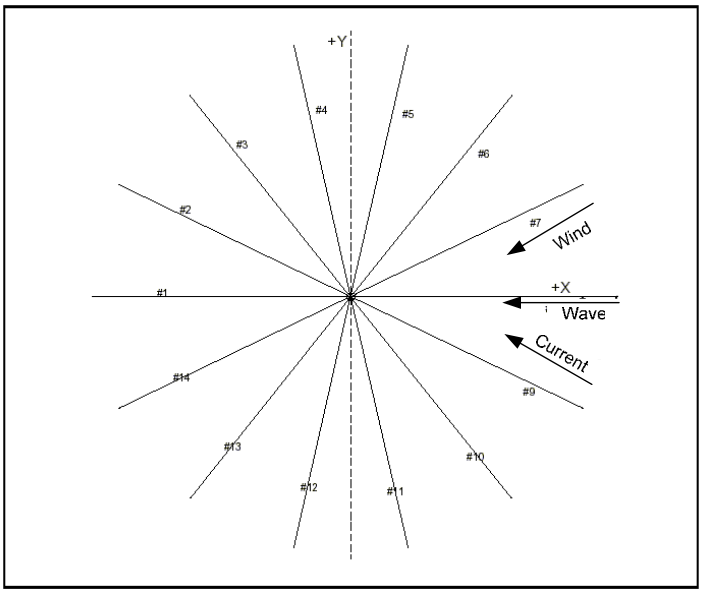

Figure 3.1: A spread mooring system

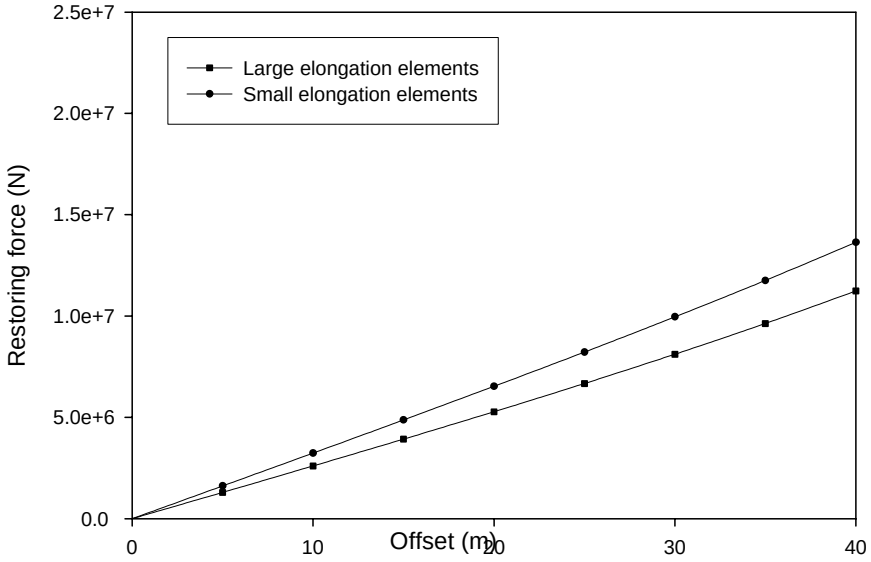

Figure 3.2: Comparison of related static offset curves (water depth 10,000 ft).

IV. Estimates of Design Loads for 100-year Hurricane in the Gulf of Mexico

The model parameters assumed for the theme spar are summarized in Table 4.1. In the case of the spar positioned by a steel mooring system in 3,000 ft water, the predictions given by COUPLE were compared with the corresponding measurements of the model tests and satisfactory agreement was observed (Ding et al. 2003).

Table 4.1. Hydrodynamic force coefficients.

	Normal drag coefficient	Added-mass Coef.	Viv Lifting Force Coef.	Strouhal Number
Spar	1.16	1.00	0.45	0.2
Chain	2.45	1.40	N/A	N/A
Rope	1.20	1.00	N/A	N/A

The amplitude spectra surge, sway and heave of the hull under the impact of a 100-year hurricane of (H_s=12m and T_p=14s) in the Gulf of Mexico were obtained using COUPLE. As an example, the surge amplitude spectrum is shown in Figure 4.1. The surge and sway are dominated by the slow-drift motion. Typical amplitudes of the slow-drift surge range from 4 m to 8.5 m and those of sway from 2 m to 4 m. The amplitudes of the heave range from 1 m to 2 m. The average periods of the slow-drift surge and sway are similar, about 190 s, and that of heave is about 30 s, which are close to the corresponding natural periods determined by numerical simulation of free decay tests of the spar.

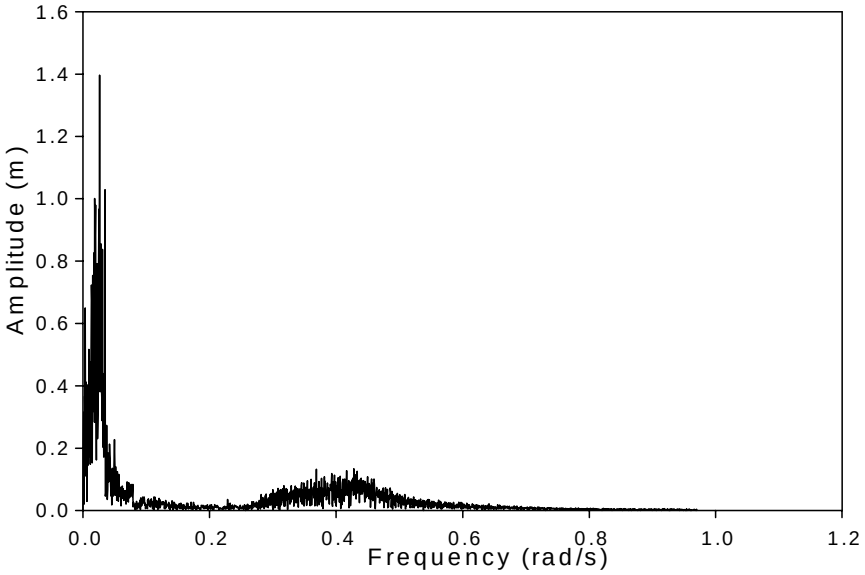

Figure 4.1: Surge amplitude spectrum

To provide an overall picture of a three-hour storm simulation, we summarize the statistics of the global motions of the hull in 3,000 ft water in Table 4.2.

Table 4.2. Statistics of the global motions of the hull in 3000-ft water.

	Mean	Standard Deviation	Max
Surge (m)	-1.78E+01	2.43E+00	2.57E+01
Sway (m)	-2.44E+00	1.81E+00	6.86E+00
Heave (m)	-1.19E-01	5.59E-01	2.46E+00
Roll (degree)	9.63E-01	8.11E-01	3.53E+00
Pitch (degree)	-3.29E+00	1.73E+00	1.17E+01
Yaw (degree)	-2.10E-02	1.155E-01	7.0E-02

The maximum tension of each individual mooring line occurs at its fairlead. The maximum tension in all mooring lines seems dominated by the slow-drift surge and sway of the hull. However, the tension caused by the heave of the hull is also significant. For the study of the force applied on the caisson, our main concerns are the tensions of each mooring line and its angle with respect to the seabed at the mudline. Considering that the most loaded mooring line is #8 (weather side), we present the tension and angle of lines #8 in 3,000 ft water as a function of time in Figures 4.2 and 4.3. Consistent with their maximum tensions at the fairlead, the maximum tension of line #8 at the mud line is the greatest among all lines. In addition, the angle of line #8 at the mudline is also greatest.

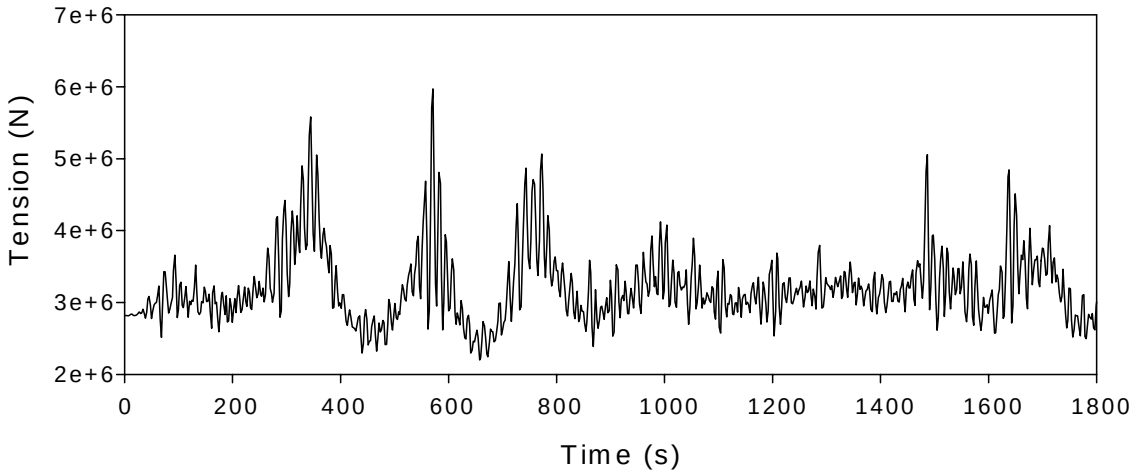

Figure 4.2: Tension of Line #8 (Weather side) at the mudline.

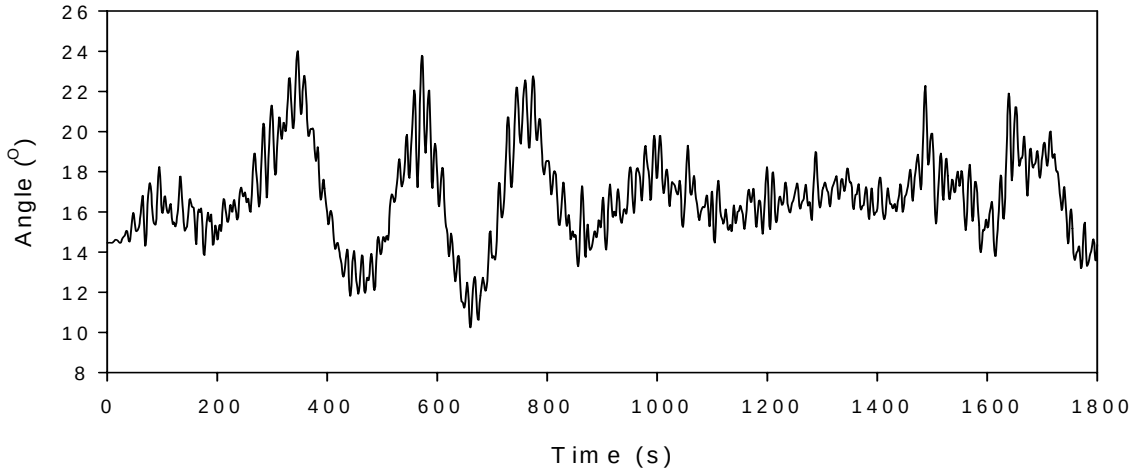

Figure 4.3: Angle of Line #8 (Weather side) with the seabed at the mud line.

To examine the dependence of the tension of mooring lines at the mudline on water depth, we present the tension spectra of line #8 at the mud line in two different water depths in Figures 4.4 and 4.5. These figures show that the tension of mooring lines at the mudline is dominated by the slow-drift surge, sway and heave motions of the hull. The comparison of the corresponding spectra also reveals that the tension in the wave frequency reduces with the increase in water depth.

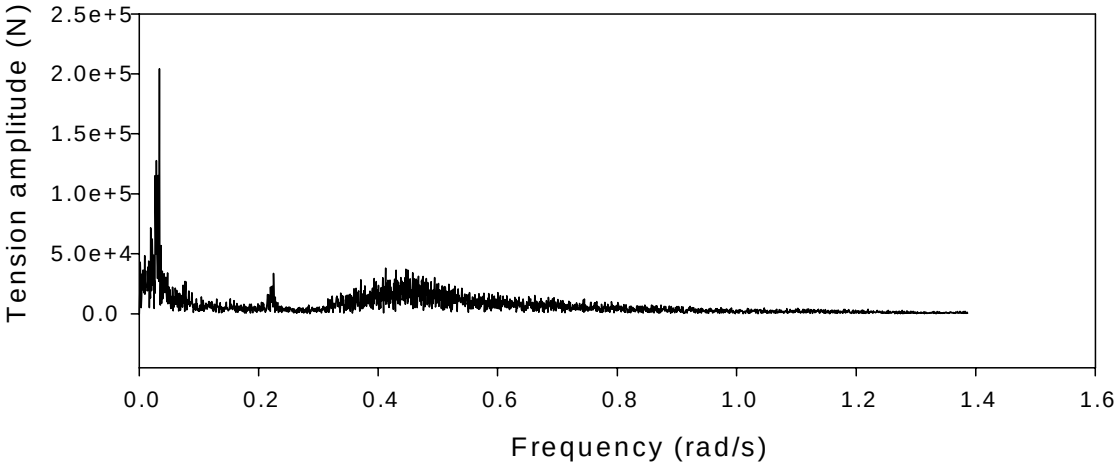

Figure 4.4: Tension amplitude spectrum of Line #8 at the mud line in 3,000ft water.

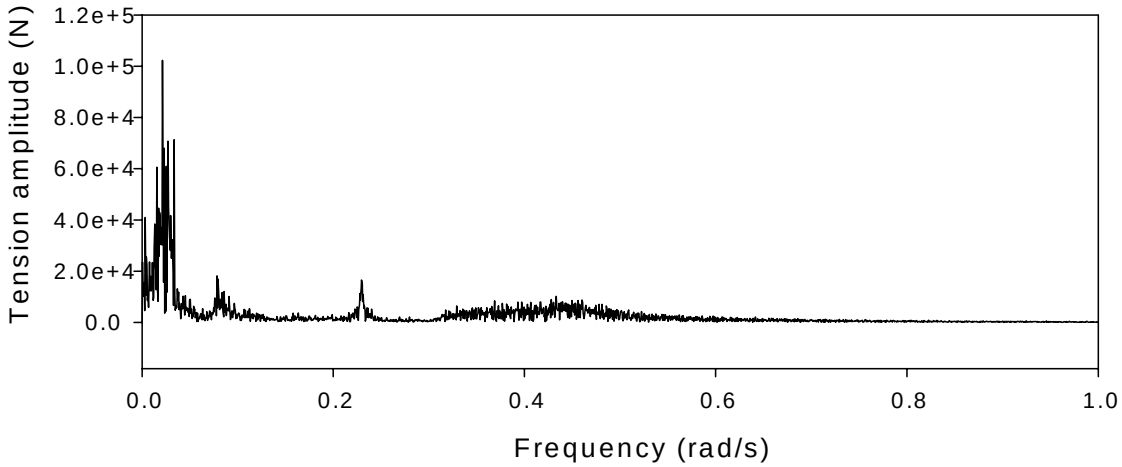

Figure 4.5: Tension amplitude spectrum of Line #8 at the mud line in 10,000ft water

V. Probability Distribution for Maximum Line Loads

In this section, the methodology used to establish a probability distribution for the maximum line loads during a storm event is summarized. This methodology consists of the following steps:

1. Determine the probability distribution of the maximum line load in a given storm event;
2. Determine the uncertainty in mean maximum line load due to uncertainty in the sea states that the spar is subjected to in its lifetime; and
3. Determine the uncertainty in the mean maximum line load due to uncertainty in the model parameters that are used in the COUPLE model.

These steps are described below using the load at the fairlead for a single line in the mooring system in the case that the mooring system is intact. However, the methodology

is general and can be used to determine the probability distribution for the maximum load (and its corresponding angle) at the mudline or the padeye of the anchor and for different cases, such as a damaged mooring system.

5.1 Maximum line load in a given storm event

Tension load simulations of the mooring anchor system were generated by the COUPLE program for 3-hour storm durations with a given sea state (Fig. 4.2). These simulations were then processed as follows to estimate the expected maximum load value and its standard deviation. The storm duration was divided into smaller intervals. Then, the maximum value from each interval was determined. Finally, the mean of these maximum values was plotted versus the interval size, as shown on Figure 5.1. The basis for this plot is an assumption that the variation of line loads with time behaves approximately according to a Gaussian process (e.g., Vanmarcke, 1983). The linearity of the data on this plot is significant because a single 3-hour storm simulation, which is the industry standard, can be used to estimate the mean value for the maximum load in a 3-hour storm by processing the simulation in smaller intervals. Otherwise, it would be necessary to estimate the mean value from a single point (there is only one maximum in a 3-hour simulation), which would not be reliable. A similar analysis is conducted to estimate the standard deviation of the maximum load. For the case shown on Figure 5.1, the corresponding coefficient of variation (standard deviation divided by mean), which represents the variability in maximum loads between 3-hour storm events, is 0.05.

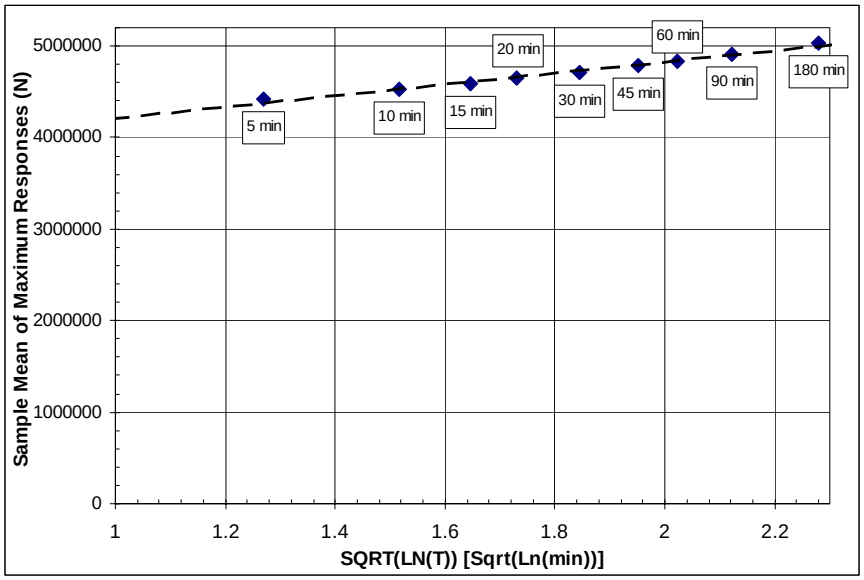

Figure 5.1: Processed simulation data to estimate mean of maximum load (line #8 at fairlead, 3,000-ft water depth, H_S= 9.32 m and T_p = 12.64 s).

5.2 Probability distribution of sea states

A probabilistic distribution for the met-ocean parameters characterizing a storm in the Gulf of Mexico was adopted from Winterstein and Kumar (1995):

1. The *significant wave height* (H_S) has been modeled as a truncated Weibull distribution.
2. The *peak spectral period* (T_p) is modeled as a conditional normal distribution with a constant c.o.v. and a mean value that depends on H_s.
3. The *surface current velocity* (V_S) is modeled as a linear function of H_S.
4. The *one hour mean wind speed* (v_w) is also modeled as a linear function of H_S.

Therefore, the hurricane is characterized completely by two parameters: H_s and T_p. In addition, hurricanes at the spar location in the Gulf of Mexico were assumed to occur independently with an annual rate of occurrence, ν, of 0.1 per year.

Using this information, a joint probability distribution of H_S and T_p can be developed that includes both the likelihood of different combinations of H_s and T_p in a hurricane as well as the frequency of hurricanes. This joint probability distribution is expressed as a reliability contour on Figure 5.2. For each contour in this figure, the volume of the joint probability distribution outside of a tangent line to the contour has a constant value. For the 50-year contour, this volume or probability is 1/50 in a one-year period. For the 100-year contour, this probability is 1/100 in a one-year period. These contours, which will be referred to as annual reliability contours, are useful because they express the distribution for H_s and T_p in terms related to the return periods specified in design guidelines.

For the reliability analysis, we are concerned about the response of the structure to storms occurring during its design life. The design life of the theme spar was assumed to be 20 years. Therefore, the annual reliability contours have been converted (assuming storm occurrences follow a Poisson process) into 20-year reliability contours on Figure 5.3. Here, the probability of being outside of a tangent line along the contour in a 20-year period corresponds to complement of the percentile. For example, this probability is 5 percent for the contour labeled 95th percentile.

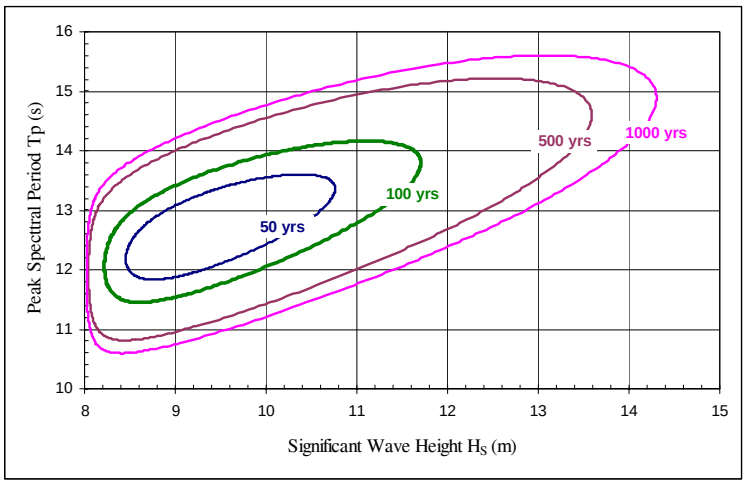

Figure 5.2: H_S-T_p annual reliability contours.

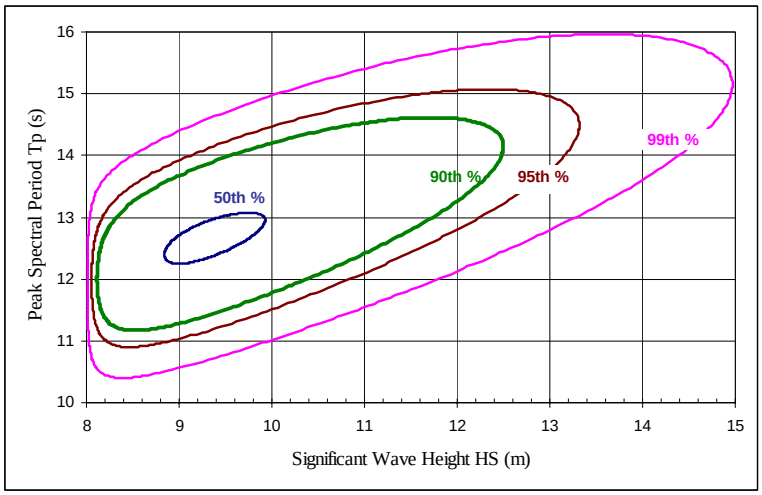

Figure 5.3: H_S-T_p reliability contours for a 20 year design life.

5.3 Probability distribution of mean maximum line loads

A probability distribution for the maximum line loads in a 20-year design life can be obtained by combining the information on the maximum line load during a given 3-hour storm (Section 5.1) with the probability distribution for the occurrence of different storm events (Section 5.2).

Three hour storm simulations were carried out with COUPLE for a large number of possible sea states, and the expected maximum loads during a 3-hour storm were estimated using the approach depicted on Figure 5.1. Figure 5.4 shows the results of this analysis. The expected maximum load contours on this plot have a nearly vertical trend, indicating that the loads on this structure during a storm event depend mostly on the significant wave height of the sea state.

Figure 5.5 combines Figures 5.3 and 5.4 and shows the load contours and the H_S-T_p likelihood contours on the same graph. Figure 5.5 can then be used to establish the probability distribution for the expected maximum load: the 50^{th} percentile value s 5,155 kN; the 90^{th} percentile value is 6,500 kN; and the 95^{th} percentile value is 7,515 kN. A lognormal distribution provides a reasonable and convenient fit to these percentiles: the median value for the mean maximum load is 5,100 kN and the coefficient of variation (c.o.v.) is 0.23.

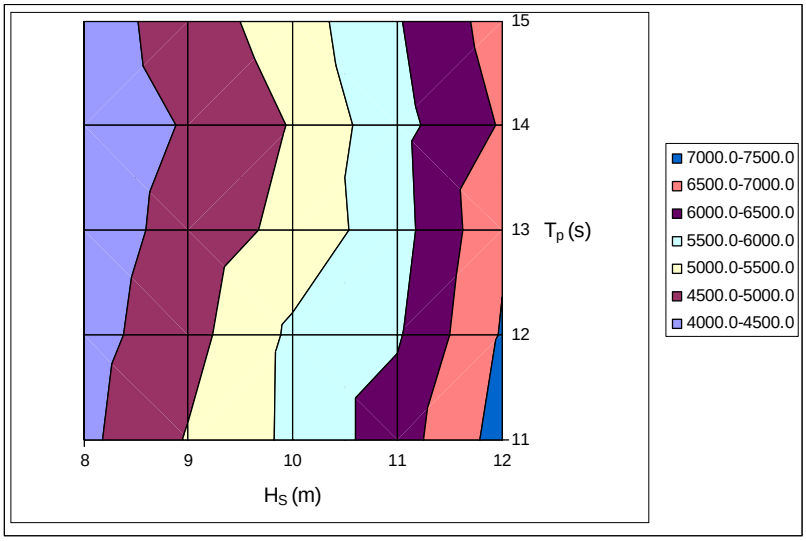

Figure 5.4: Expected maximum load (in kN) during a 3-hour storm.

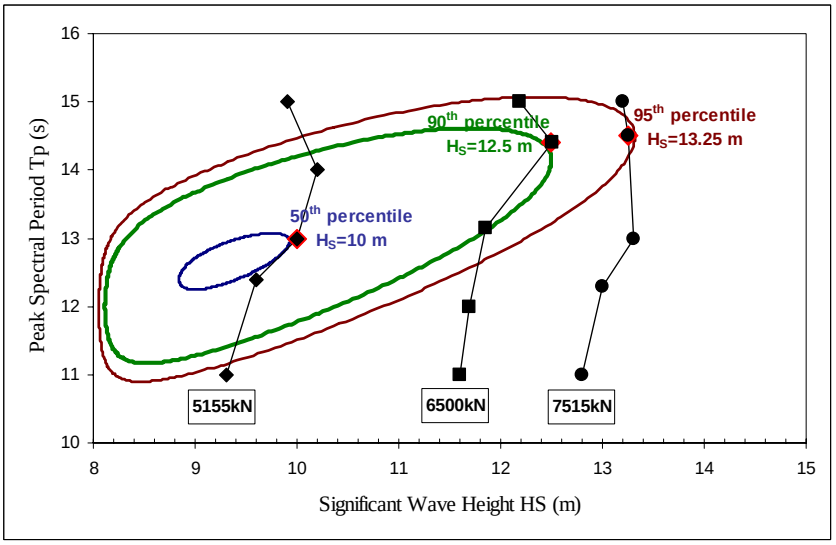

Figure 5.5: Superposition of Figures 5.3 and 5.4.

5.4 Uncertainty in model parameters

The five most significant model parameters affecting the response of the structure are the drag force coefficient, C_D the added mass coefficient, C_M the VIV lifting force coefficient, C_L Strouhal number, St, and the shape coefficient due to wind loads, C_S. Since the exact values for these model parameters are not known for the theme spar, a first-order analysis was conducted to determine how significant this source of uncertainty is on the maximum line load. To study the effect of the parameters on the maximum load, each of these parameters was varied keeping the values of other parameters fixed. The storm simulations were carried out for the sea state: H_S = 9.32 m and T_p = 12.64 s. The sensitivity of the maximum load to each parameter was calculated as a percentage change in the maximum load due to a percentage change in the model parameter. The results are

shown on Figure 5.6. In addition, an estimate was made for the c.o.v. value to reflect the magnitude of uncertainty in each parameter. These c.o.v. values and the sensitivities were then used to approximate the standard deviation in the maximum line load due to model uncertainty.

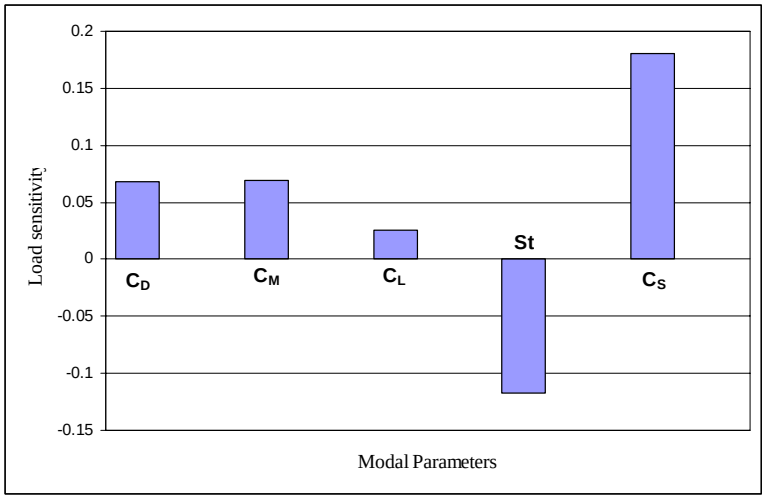

Figure 5.6: Sensitivity of the maximum load to the variation in model parameters.

5.5: Overall uncertainty in maximum line loads

The total uncertainty in the maximum line loads results from variations in maximum loads between individual 3-hour storm events (Section 5.1), variations in the mean maximum load due to variations in the metocean environment over a 20-year design life (Section 5.3), and uncertainty in the mean maximum load due to uncertainty in the response model (Section 5.4). These three sources of uncertainty are depicted in Figure 5.7; the uncertainty due to the metocean environment is the dominant source of uncertainty for this structure.

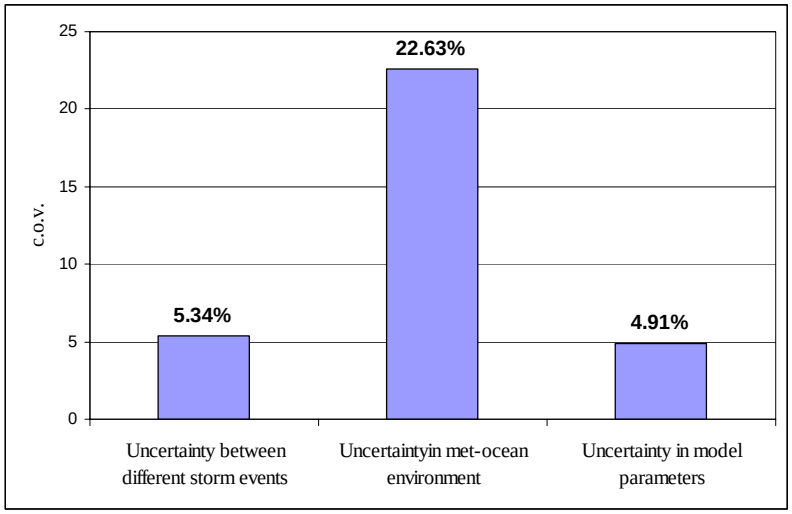

Figure 5.7: Comparison of uncertainties in the storm loads.

VI. Reliability Analysis for Mooring System

The reliability analyses for the components in the mooring system (individual lines and anchors) and for the entire system are summarized in this section.

6.1 Component Reliability

An example reliability analysis for the line that is expected to have the maximum load applied to it from a hurricane (line #8) is shown on Figure 6.1. The distribution for the maximum load at the fairlead over a 20-year design life is obtained as described in Section VII. The distribution for the capacity is obtained from the design capacity and published information on the variability in line capacity about the design capacity (e.g., Bruen et al. 1991). The probability that the load exceeds the capacity in the design life is $1x10^{-5}$. This probability of line failure is significantly smaller than published target values that are several orders of magnitude higher (e.g., Goodwin et al. 2000).

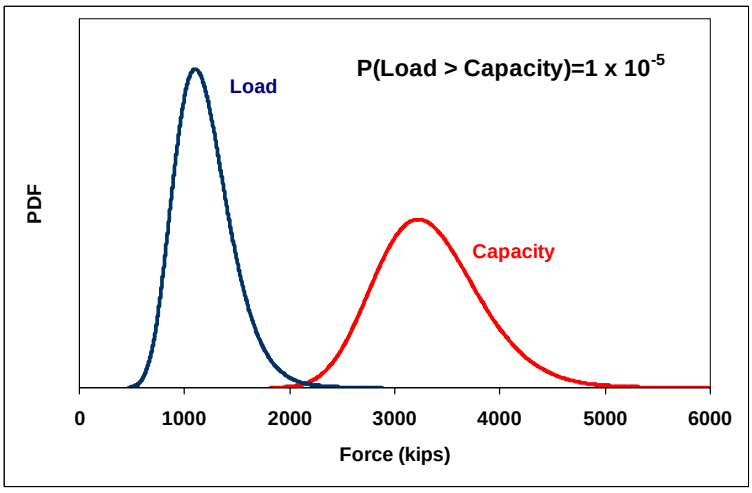

Figure 6.1: Reliability analysis for a single line.

A similar analysis has been conducted for the line anchor (a suction caisson foundation), and the probability of failure for the line at the fairlead and at the anchor are shown on Figure 6.2 as a function of the factor of safety used to design the anchor. The conventional factor of safety for the anchor is around 2.0. This graph shows that this factor of safety could be lowered to less than 1.5 and still provide more reliability in the anchor compared to the line.

One additional consideration in the reliability of the anchor is the effect of a minimum possible capacity. If there the minimum capacity is zero, then the curve labeled "R_{min}/R_{med} = 0.0" in Figure 6.2 applies. However, the minimum capacity for a suction caisson can be on the order of 40 to 50 percent of the design (or median) capacity, can have a significant effect on reducing the probability of failure. Note that for typical values for the lower-bound capacity, factors of safety close to 1.0 could be used for the anchor (in the damage case) and still provide for a comparable level of reliability as for the line itself.

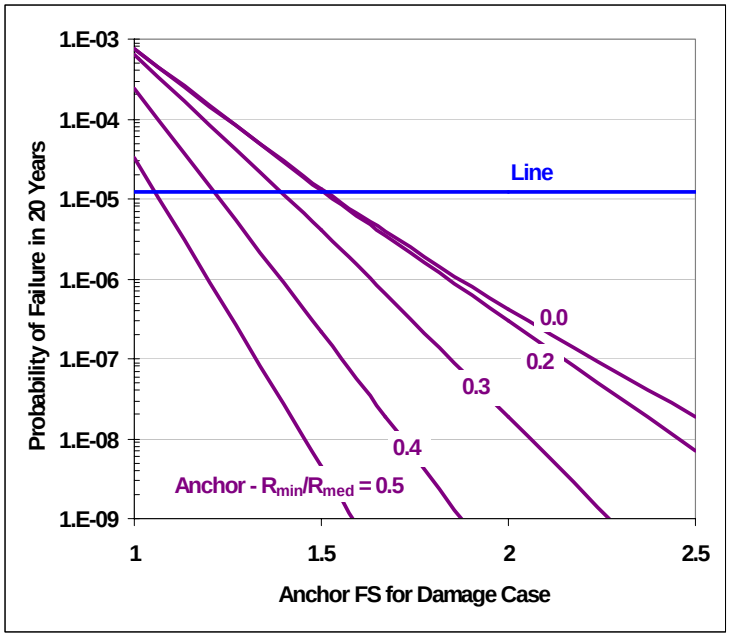

Figure 6.2: Comparison of line and anchor reliability (R_{min} is minimum possible capacity and R_{med} is median capacity).

6.2 System Reliability

The reliability of the mooring system is defined as the probability that station keeping will be maintained over the 20-year design life. It is assumed that the loss of two mooring lines (either in the line itself or in the anchor) will lead to a loss of station keeping. This section describes the status of ongoing work in evaluating the system reliability.

The methodology to evaluate the system reliability involves updating the distribution for H_s given that one of the lines has failed during the storm. Since the maximum load is expected on line #8, the distribution for H_s is updated given that line #8 has failed. Figure 6.3 shows this approach. The blue curve on Figure 6.3 is the original (before knowing that line #8 has failed) probability distribution for H_s. The pink curve on Figure 6.3 is the probability that line #8 will fail as a function of H_s. These two curves are multiplied together to produce the updated probability distribution for H_s given that line #8 has failed (the green curve on Figure 6.3). Note that the updated probability distribution for H_s is shifted to the right to reflect the greater likelihood that a severe storm has occurred if line #8 has failed.

The next step in the methodology is to establish the load on the most-heavily loaded line if line #8 fails, which is line #9. Results obtained from COUPLE analyses on the theme spar are plotted on Figure 6.4.

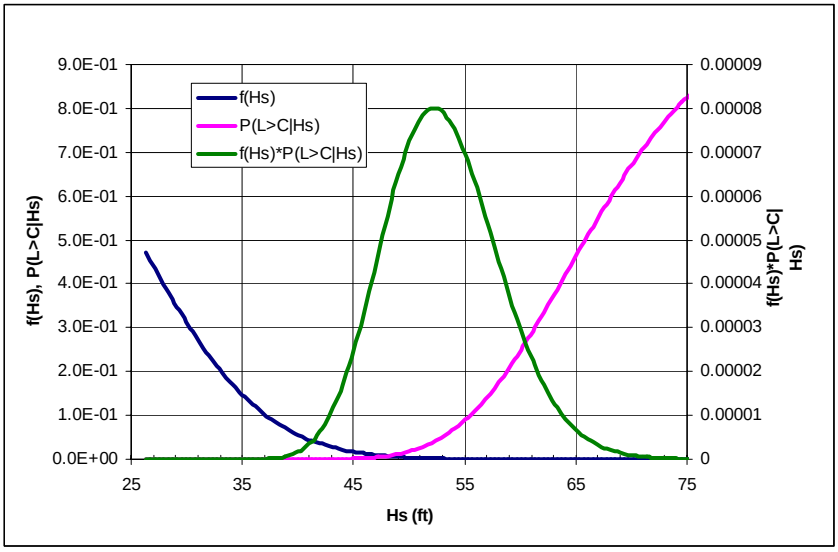

Figure 6.3: Probabilities of sea state and failure for mooring line #8.

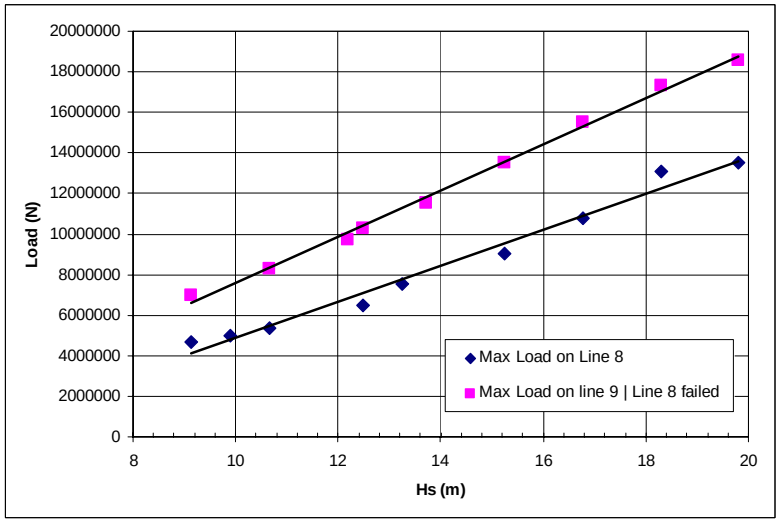

Figure 6.4: Expected maximum load at fairlead for mooring lines #8 and #9 plotted against the significant wave height.

Combining the information on Figures 6.3 and 6.4, the updated probability distribution for the maximum load on line #9, given that line #8 has failed, can be obtained. With this updated distribution for the maximum load on line #9, the probability that line #9 fails given that line #8 has failed can be calculated. This probability provides an indication of the redundancy that is available in the mooring system. If it is equal to 1.0, then there is no redundancy because line #9 will fail if line #8 fails and the spar will lose station keeping. A redundancy factor, defined as the inverse of this conditional probability, is therefore used to measure the system redundancy. This redundancy factor is shown on Figure 6.5 (the green curve) as a function of the factor of safety used to design each individual mooring line. A factor of safety between 1.5 and 2.0 is typically used for the line. For comparison purposes, the blue on Figure 6.5 curve shows an upper bound on the possible redundancy. This

curve corresponds to a mooring system where there are two line #8's; the first line takes all of the load until it fails, and then the second line picks up load.

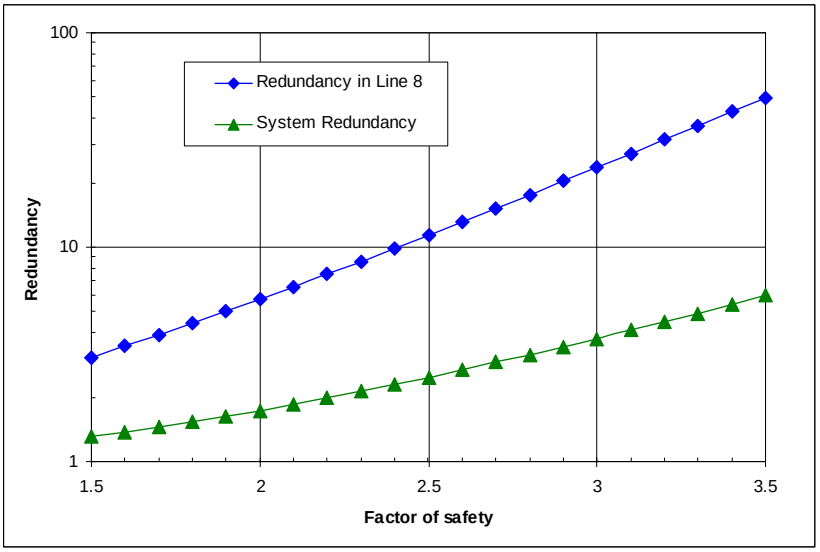

Figure 6.5: Mooring system redundancy factor versus factor of safety for line design.

VII. Summary

The major conclusions that have been reached thus far in this ongoing work are:

1. The reliability of an individual mooring line in this theme spar is well-above target reliabilities that have been published and generally accepted by industry.
2. The reliability of the line anchor is significantly higher than that for the line itself.
3. There is redundancy in the mooring system during a severe storm event; the probability of failure for the mooring system given that the most heavily loaded line has failed is on the order of 50 percent.

VIII. Present Work

Work in 2004-2005 is focusing on conducting similar analyses for loop currents.

References

API RP-2A, (1997). Recommended Practice for Planning, Designing and Constructing Fixed Offshore Platform. American Petroleum Institute, Washington, DC.

Bosman, R. L. M., and Hooker, J. (1999). Elastic modulus characteristics of polyester mooring ropes. Proceedings of the Annual Offshore Technology Conference, v3, 139-143.

Bruen, F. J., Gordon, R. B. and Vyas, Y. K. (1991), "Reliability of a Deepwter Gulf of Mexico FPS Spread Mooring," Proceedings of OMAE, 179-186.

Cao, P.M. and Zhang, J. (1997). Slow motion responses of compliant offshore structures. International Journal of Offshore and Polar Engineering 7(2), 119-126.

Chen, X.H., Zhang, J. and Ma, W. (1999). Coupled Analysis of a JIP Spar and Its Mooring System. Proceedings of the International Offshore and Polar Engineering Conference (ISOPE) Vol. I, 293-300

Chen, X.H., Zhang, J., Johnson, P. and Irani, M. (2001a). Studies on the dynamics of truncated mooring line. Proceedings of the International Offshore and Polar Engineering Conference (ISOPE), Vol.2, pp. 94-101.

Chen, X.H., Zhang, J, and Ma, W. (2001b). On dynamic coupling effects between a spar and its mooring lines. Ocean Engineering 28, pp. 863-887

Chen, X., Zhang, J., Liagre, P., Niedzwecki, J. and Teigen. P. (2002) Coupled Dynamic Analysis of A Mini TLP: Comparison with Measurements. 21st International Conference on Offshore Mechanics and arctic Engineering, OMAE 02-8536.

Del Vecchio, C.J.M. (1992). Light weight material for deep water mooring. Ph D. thesis, University of Reading, UK.

Ding, Y., Kim, M., Chen, X. and Zhang, J (2003). Coupled Analysis of Floating Production System. Deepwater Mooring Systems Concepts, Design, Analysis, and Material. Houston, Texas, 152-167.

Garrett, D.L., (1982). Dynamic analysis of slender rods. Journal of Energy Resources Technology, Transaction of ASME 104, 302-307.

Goodwin, P., Ahilan, R. V., Kavanagh, K. and Connaire, A. (2000), “Integrated Mooring and Riser Design: Target Reliabilities and Safety Factors,” Proceedings of OMAE, 185-792.

Lee, C.H. (1995). WAMIT Theory Manual. Report No. 95-2, Massachusetts Institute of Technology, Cambridge, Massachusetts.

Kim, MS, Ding, Y. and Zhang, J (2003). Dynamic simulation of Polyester Mooring Lines. Deepwater Mooring Systems Concepts, Design, Analysis, and Material. Houston, Texas, 101-114.

Ma, W. and Webster, W.C. (1994). An Analytical Approach to cable Dynamics: Theory and User Manual. SEA GRANT PROJECT R/OE-26.

Sarpkaya, T. and Isaacson, M., (1981). Mechanics of Wave Forces on Offshore Structures. Van Nostrand Reinhold Company Inc., New York.

Tuah, H. and Hudspeth, R.T. (1982). Comparison of numerical random sea simulations, Journal of Waterway, Port, Coastal and Ocean Divisions, ASCE, 108, (WW4), Proceedings Paper 17488, pp. 569-584.

Vanmarcke, E. H. (1983), Random Fields: Analysis and Synthesis, The MIT Press, Cambridge, Mass.

Winterstein, S. R. and Kumar, S. (1995). Reliability of Floating Structures: Extreme Response and Load Factor Design, Offshore Technology Conf., OTC 7758, Houston, Tex., pp569-578.

Zhang, J., Chen, L., Ye, M. and Randall, R.E. 1996. Hybrid Wave Model for Unidirectional Irregular Waves. Part I. Theory and Numerical Scheme, Applied Ocean Research, Vol. 18, 77-92.

Zhang, J., Yang, J., Prislin, I., Wen, J., and Hong, K. 1999. Deterministic Wave Model for Short Crested Ocean Waves, Part I. Theory and Numerical Scheme. applied ocean Research, Vol. 21, 167-188.